Contents lists available at ScienceDirect

Waste Management

journal homepage: www.elsevier.com

Blend design tools for Medium Combustion Plants (MCP) firing biomass wastes

I. Ibarra[a,*], G. Aragón[a], I. Gómez[a], I. Múgica[a], J. González[a], J. Rodríguez Maroto[b], E. Rojas[b], D. Sanz[b], R. Ramos[c], R. Escalada[c], E. Borjabad[c], C. Gutiérrez-Canas[a]

[a] *Dpt. Chem. & Environ. Eng., University of the Basque Country UPV/EHU, Alda. de Urquijo s/n, 48013 Bilbao, Spain*
[b] *CIEMAT Avda. Complutense 40, 28040 Madrid, Spain*
[c] *CEDER-CIEMAT, Autovía de Navarra A15, Salida 56, 42290 Lubia, Soria, Spain*

ARTICLE INFO

Article history:
Received 18 May 2017
Received in revised form 30 October 2017
Accepted 31 October 2017
Available online xxx

Keywords:
Waste biomass combustion
Thermodynamic prediction
Fuel blending criteria
Fouling
Slagging
Fluidized bed combustion

ABSTRACT

A feasible alternative for agricultural or forestry waste management is the operation of a distributed network of sustainable Medium Combustion Plants (MCPs). However, one of the main factors that hinder its development is the propensity to operational problems derived from corrosion, slagging and fouling characteristics of both bottom and fly ashes. Therefore, a cost-effective approach for these multi-product MCP could be based on predictive tools for an optimal formulation of a fuel blend. This work focuses on the assessment of the ability of these methods to provide guidance for preventing ash-related operational problems and to provide fuel-blending rules.

The more widespread tools pertain to two types: compositional classification based on chemical analysis of laboratory ashes, and thermodynamic prediction of the most likely species and phases. Both criterion numbers and compositional maps are ranking methods based on the chemical analysis at a given ashing temperature. Thermodynamic equilibrium modeling is not constrained by any difference in the physical conditions of the MCP compared to those in the laboratory.

Both kind of prediction tools have been validated in an MCP firing olive tree pruning residues as well as its typical blends in order to mimic a plausible pattern of fuels along a full year operating campaign. An intensive experimental campaign encompasses plant monitoring and off-line analysis of the ashes along the process line.

Interpretation of compositional plots has revealed to be potentially sensitive to ashing temperature. Here are presented examples showing how this variable could lead to either insignificant differences or to a substantial disparity in the a priori fuel diagnosis.

Some inconsistencies have been observed between the predictions based on criterion numbers, even for the same fuel and for ranking rules specifically formulated for biomasses. Moreover, it does not match consistently with the information obtained from phase diagrams. Therefore, their use should be limited to the case of a well-established selection of a fuel index for a well-defined fuel provided empirical evidence of an enough good description of the ash behavior, which is not the most frequent case.

Abbreviations: A, fuel component: composted fraction of sewage sludge; A′, triangular diagram compositional point for A process ashes; AC, blend of components A and C; AC′, triangular diagram point for blend AC process ashes; ACs, triangular diagram compositional point for AC simulation; B,, fuel component: fraction of municipal solid waste; B′, triangular diagram compositional point for B process ashes; BC, blend of components B and C; BC′, triangular diagram point compositional for BC process ashes; BCs, triangular diagram point compositional for BC simulation; BF, bag Filter; C,, case fuel: olive tree pruning waste; C′, triangular diagram point compositional for C process ashes; Cs, triangular diagram point compositional for C simulation; ESP, electrostatic precipitator; FB, fluidized bed; FC, fixed carbon; G, mole of gaseous species at T; HF, hybrid filter; HHV, high heating value; ICP/MS, inductively-coupled plasma/mass spectrometry; ICP/AES, inductively-coupled plasma/atomic emission spectroscopy; LHV, lower heating value; MCP, medium combustion plant; RH, relative humidity; S, total molar amount of solid species; STGE, scientific group thermodata Europe; T, temperature; VM, volatile matter; XRD, X-ray diffraction; XRF, X-ray fluorescence

* Corresponding author.
Email address: iibarra011@ikasle.ehu.eus (I. Ibarra)

https://doi.org/10.1016/j.wasman.2017.10.052
0956-053/

Thermodynamic equilibrium calculations allow a more precise prediction of the main species in the condensed phase, without the constraint of the ashing temperature. Elemental closure of main ash-forming elements with the chemical analysis of the process ashes presents small differences, and their proximity localization on the phase diagrams denote similar prediction between predicted and process ashes.

1. Introduction

Mediterranean countries produce 95% of the total world olive oil with important environmental, social and economic implications. Olive tree pruning residue is an important resource in the Mediterranean Basin, where basically the 8.6 million hectares of olive trees grown worldwide are located (FAOSTAT, 2009). Spain ranks first in the olive global production with $7.2 \cdot 10^6$ t, which becomes 37% of this production (Red Española de compostaje, 2015). The estimated yield of pruning residue widely ranges from 0.3 t/ha, based on an average of 120 trees/ha and 25 kg dry pruning per tree, to 1 dry ton/ha (Spinelli and Picchi, 2010) to 3 t/ha year (Red Española de compostaje, 2015). The use of olive tree pruning residue as an energy resource is growing and strongly depends on the local development of systems for collection, processing, and delivery as well as on the feasibility of blends to ensure the operation on a yearly basis (Aragon et al., 2015). Its use as domestic grade in the form of pellets is becoming popular, so the requirement of a low ash content for this use causes a further waste fraction of downgraded characteristics, although still able to be valorized in an industrial facility. The seasonal supply variability leads to this pruning waste to be blended with customary local components while keeping the nominal thermal output of the MCP. In addition to the characteristic seasonality in supply, which leads to a traditional practice of blending with other fuels, there is a growing interest on "fuel engineering" to minimize corrosion and fouling as well as "end-of-life", and to prevent atmospheric emissions. The so-called "fuel engineering" (Boström et al., 2012, 2009b, Grimm et al., 2012, 2011; Lindström et al., 2007; Piotrowska et al., 2012, 2010; Steenari et al., 2009; Steenari and Lindqvist, 1998; Xiong et al., 2008), that is, the purposely-optimized inorganic content of the fuel, relies on user-friendly reliable tools for prediction and mitigation of critical ash and emission related issues.

Decentralized networks of MCP (1–50 MWth) are a promising choice in agricultural waste management, not only for logistic reasons but also for its ability to fulfill the requirements of a number of distributed energy applications, among them, electricity generation, domestic/residential heating and cooling, or heat/steam for industrial processes. However, some caveats related to ash behavior and fine particulate emission remain mostly unsolved.

Until now, there was a lack of emission limit values for operations with a rated thermal input less than 50 MW. However, the European MCP Directive (Directive (EU), 2015/2193, n.d.), establishing limit values for both existing and new installations will have to be transposed by Member States by December 2017. This is a strong driver for the implementation of new routine tools based on a knowledge transfer, which can guarantee both the sustainable operation of the MCP and the prevention of operational problems. FB combustion is a flexible technology that enables burning fuels of widely varying quality under easily controlled operation (Van Caneghem et al., 2012). Specifically, bubbling FB has turned into a popular technology for efficient combustion of heterogeneous fuels with high moisture and ash content.

Knowledge of the mixture influence on the properties of the final ash materials can make it possible to avoid fuel combinations with unwanted properties, or even to design an ash for a certain end-of-life application. Many kinds of biomass fly ashes (Cuenca et al., 2013) have similar pozzolanic properties to the coal fly ash, and can be added to concrete as mineral admixtures. However, this is not the case for ashes from olive wood combustion due to its characteristic low oxide content (Vassilev et al., 2010). The capacity to reduce ash-related problems is strongly influenced by the ratios between problematic reactive components in biomass ash, as well as reaction atmosphere and combustion technology. Depending on the fuel to be used, the blending criteria could be based on increasing the Al-silicates, sulfur, calcium and phosphorus content (Wang et al., 2012). Potential waste feedstocks rich in S and other elements such as Ca, P, Al and Mg, can capture released K and improve the sintering characteristics (Skoglund et al., 2013) and components with higher amounts of P, S and Si, can improve combustion properties of problematic fuels. This knowledge is still fragmentary because of the large heterogeneity of waste biomass feedstocks and its blends as well as the lack of user-friendly robust guidelines for feedstock blending.

Previous studies (Davidsson et al., 2008; Fernández Llorente et al., 2006; Kassman et al., 2013; Vamvuka et al., 2008; Wang et al., 2012) report the results of the use of additives, such as limestone and a variety of waste materials, to mitigate ash-related problems and atmospheric emissions. However, this can lead to undesired outcomes in the absence of specific knowledge of the consequences of whatever blending action on both emissions and ash characteristics. A frequent consequence of the Ca compounds is the undesired increase in KCl formation, due to the modification in the interplay between S and Cl. These Ca-silicates present higher melting temperatures than the K-silicates. Also, a higher K release is generated when the (Mg + Ca)/Si ratio is higher, demonstrating that Mg and Ca have an effect on K release (Thy et al., 2000). Knudsen et al. (2004) suggest that when the temperatures increase, Ca and Mg have stronger bonds with Si than with K, and therefore, K is available for its reaction with Cl. The high reactivity of biomass ashes compared with those from coal is frequently attributed to their high content in alkali metals and to the clear differences in the speciation of ash precursors in biomass. Although the influence of the biomass co-firing with sulfur enriched fuels on particulate emissions has been investigated (Jiménez and Ballester, 2005), little attention has been paid to the olive tree pruning case. Doshi et al. (2009) classified the inorganic content into three groups: (1) salts, (2) organically bound, and (3) minerals, either from adventitious origin or related to inclusions, which in turn can be much more reactive. However, interaction between ashes from different fuels is poorly understood and a number of trends have been reported (Hupa, 2005).

Wang et al. (2012) recommend more detailed calculations and full-scale test for the design of an appropriate fuel blend. This approach can exceed the technical capability of most of the MCPs, so a robust and simple diagnosis based on fuel engineering tools would enable plant operator a safe and sustainable MCP management.

In this work, the main goal is to assess the suitability of prediction tools, which enable a quick and robust diagnosis of the blending for an optimized MCP operation. The confirmation of fouling, corrosion and slagging propensity predictions by means of a quantification and characterization of the deposits is out of the scope of these experiments, because of requirement of long-term, single-fuel campaigns of such a study (Hansen et al., 2014). Therefore, the main outcome of the present work is the suitability assessment of the available prediction approaches for an accurate a-priori diagnosis of a given waste biomass blend.

2. Fuel engineering tools

The predictive tools used in this work for blending guidance or fuel engineering follow two different approaches: those based on chemical analysis of laboratory ashes such as criterion numbers and compositional plots or phase diagrams, and those based on a multiphase thermodynamic equilibrium forecasting, which in turn just requires the total elemental load (fuel and air) to the furnace.

2.1. Methods based on ash composition

A number of ternary diagrams of ash composition have been proposed as diagnostic tool. Fernández Llorente and Carrasco García (2005) build a ternary diagram based on three inorganic groups: SiO_2–CaO–K_2O, for ashes at 550 °C and 775 ± 75 °C. Vassilev et al. (2013b) clearly delimit the range of use of this kind of information to major ash forming elements, putting off for more extensive investigations the assessment of minor or trace elements influence. An important caveat when using these diagrams stems from the lack of information about both the equivalence ratio and the temperature when ashing in the laboratory, for the differences in diagnosis arising from the differences in conditions. This is a controversial issue, as discussed in detail later in this paper. Hupa (2005) plainly state that the quantitative prediction of the release of the ash forming matter in combustion is not possible just based on laboratory information, frequently just an elemental analysis in compliance with a standard ashing procedure. Furthermore, as pointed in Vassilev et al. (2013b), biomass ash melting characteristically occurs over a rather wide temperature range. However, the clarity of the compositional plots and the appropriate use of such a kind of tools to explore tendencies depending on the blending criteria deserve a detailed assessment in a case-by-case basis.

Vassilev et al. (2014) present a new chemical classification of inorganic matter in biomass and its ashes, based on groups formed from the most abundant oxides (Si, Al, Ca, Mg, K and P). Coupling criteria have been established according to the experimental positive and negative correlation among them. As an example of a dual behavior of an element depending on its different genetics, it is herein presented the case of Na, which can occur in both mobile (salts) and immobile (silicates) species.

The vertices of the triangle are defined coupling the ash-forming elements as follows: three groups: (1) Si-Al-Fe-Na-Ti (glass, silicates and oxy-hydroxides); (2) Ca-Mg-Mn (carbonates, oxyhydroxides, glass, silicates, phosphates and sulfates); and (3) K-P-S-Cl (phosphates, sulfates, chlorides, glass, silicates and carbonates). The diagram is divided in four areas claimed to define high, medium and low acid tendencies of biomass ash types (''S'', ''C'', ''K'' and ''CK'') and sub-types.

The prevention of these problems (slagging and fouling) is very complex for the type of biomass residues studied. As an alternative for predicting the propensity to operational problems of biomass fuels, a range of empirical criterion numbers have been proposed, mostly based on laboratory ash composition (Elled et al., 2010; Hu et al., 2011; Jenkins et al., 1998; Li et al., 2013a,b; Niu et al., 2016; Pronobis, 2005; Teixeira et al., 2012; Vamvuka et al., 2009).I It was found that some basic compounds reduce the melting temperature, while acidic ones increase it (Pronobis, 2005). Therefore, a set of criterion numbers has been proved useful in predicting coal slagging and fouling, but not directly in biomass (Niu et al., 2016). Hu et al. (2011) emphasize how the extrapolation of indexes for coal fails in predicting the slagging behavior of biomass. Given the potential benefit of these indexes, their diagnostic suitability of the more widespread ones is assessed. A brief definition of these indexes follows.

The Basic-to-Acid Ratio $R_{B/A}$ (Eq. (1a)) allocates to alkaline and earth alkaline oxides the same role in the silicate-melt formation (Jenkins et al., 1998; Vassilev et al., 2013b). The minimum value for coal is approximately 0.75, and lower for biomass fuels. The diagnosis for deposition (Vamvuka et al., 2009) is ranked as follows: low for <0.5, medium for 0.5–1 values, and high for values >1. A slightly modified definition (Pronobis, 2005) including the P content is claimed to closer suit the characteristics of biomass fuels (Eq. (1b)). This element has an important influence on ash fusibility and slagging and fouling properties. Pronobis (2005) present this index, where the P_2O_5 content is located in the numerator, because it produces an ash melting temperature drop although it can be an acid component.

$$R_{B/A} = \frac{\%(Fe_2O_3 + CaO + MgO + K_2O + Na_2O)}{\%(SiO_2 + TiO_2 + Al_2O_3)} \tag{1a}$$

$$R_{B/A(+P)} = \frac{\%(Fe_2O_3 + CaO + MgO + K_2O + Na_2O) + \%(P_2O_5)}{\%(SiO_2 + TiO_2 + Al_2O_3)} \tag{1b}$$

Slag viscosity index (Pronobis, 2005) (Eq. (2)) is proposed to distinguish between the rank of high viscosities (>72) and supposedly low slagging tendencies, and those of high slagging propensity (<65).

$$S_R = \frac{\%(SiO_2)}{\%(SiO_2 + Fe_2O_3 + CaO + MgO)} \cdot 100 \tag{2}$$

Fouling probability index (Eq. (3)) is based on the basic-to-acid ratio and claimed to be more appropriate for biomass combustion (Teixeira et al., 2012) since it captures the relevance of alkali elements as the main fouling drivers. The formation probability is allocated as low for values <0.6 and extremely high for values >40.

$$Fu = R_{B/A} \cdot (\%K_2O + \%Na_2O) \tag{3}$$

Finally, the Cl and S ratios (Eq. (4a) and (4b)) have been shaped from field studies on utility boilers and small scale furnaces (Elled et al., 2010). Some of the essential elements (Si, Al, K, Cl, and S) that influence alkali transformations and trigger alkali-induced slagging are included. Slight slagging is expected for Cl ratio and S ratio lower than 1.0 and 0.5, respectively. High slagging tendency is indicated by Cl ratio and S ratio ranging within 1.0–2.4 and 0.5–1.9, respectively (Niu et al., 2016).

$$\text{Cl ratio} = \frac{\%(Cl + K_2O + Na_2O)}{\%(SiO_2 + Al_2O_3)} \tag{4a}$$

$$\text{S ratio} = \frac{\%(S_{Volatile} + K_2O + Na_2O)}{\%(SiO_2 + Al_2O_3)} \tag{4b}$$

The % of volatile S is the sulfur available in the biomass that is oxidized to SO_2. Therefore, if only S and alkali content increases, slagging and fouling problems also increase. In this case, it has been calculated for the total S content in the biomass, considering that the full S content is oxidized to SO_2 (Niu et al., 2016).

These kind of numbers have been criticized for a number of reasons, among them (Vassilev et al., 2015), because they are unable to deal with the presence of refractory or fluxing minerals and species in the inorganic matter, identified as one of the more important causes to operational troubles. As a further refinement, it has been proposed (Zevenhoven-Onderwater et al., 2000) a modified approach by combining the results of a chemical fractionation analysis of the fuel, distinguishing the reactive and non-reactive inorganic fraction, with a simplified equilibrium approach. Khadilkar et al. (2016) combine the use of ranking indexes with thermodynamic modeling of chemical subsets. These more sophisticated approaches have not been followed in this work, because of their intermediate status between a fast and rough estimate and a comprehensive multiphase modeling.

2.2. Methods based on thermodynamic equilibrium

In an MCP context, the intrinsic lack of tests and analysis requirements make the chemical multiphase equilibrium calculations affordable and cost-effective (Piispanen et al., 2012). They are based on the minimization of the total free Gibbs energy of the system under a mass balance constraint. Skrifvars et al. (1998) report prediction on the melting temperature of different ashes by means of a simplified equilibrium model. Gilbe et al. (2008) applied a thermodynamic equilibrium hypothesis to a subset of major components in small scale appliances, together with further experimental validation. This approach, although extensively used (Goñi et al., 2003; Johansen et al., 2011; Miller et al., 2002a,b; Moradian et al., 2015; Nutalapati et al., 2007; Poole et al., 2008), has some important limitations even in the case of a comprehensive elemental matrix and reaction scheme. For equilibrium calculations, perfect mixing is considered, kinetic limitations and rate processes are ignored and, in many cases, condensed phases are assumed to behave as ideal ones. However, reliable results can be obtained considering simultaneously heterogeneous chemical kinetics, multiphase equilibrium models, and the presence of a melt phase at the ash forming matter (Boström et al., 2012). Thus, this work includes data about complex and non-ideal solid phases, such as silicate slags, already available in thermo-data bases. In any case, the search of user-friendly tools should consider either comprehensive or subset thermodynamic models as a further step in the optimization of MCP operation through fuel engineering.

In this work, multiphase chemical equilibrium composition was predicted by chemical equilibrium calculations code MTDATA (Davies et al., 2002), using the MULTIPHASE software module and STGE (Scientific Group Thermodata Europe) database. Detailed descriptions of the thermodynamic equilibrium methods are available elsewhere (Miller et al., 2003; Miller et al., 2002a,b).

The MULTIPHASE module can solve equilibrium problems that include a large number of phases and components. Given a composition, temperature and pressure (or volume) of the system, this module calculates the steady state in terms of distribution of components and species between stable phases. It also allows the inclusion of composition, temperature, pressure or volume, partial pressures and activities in a single variable. Depending on the nature of the problem, one or two stages of calculations can be used. The first one uses a method to determine equilibrium when all components and phases are $>10^{-6}$ mol. The second stage establishes chemical balance programs to generate greater accuracy in small quantities of species when each thermodynamic component has an established and independent activity in the system.

This package was selected due to its ability to describe the behavior of the K-P-Ca system. Recently, this approach has been used and validated for the case of thermal processing of sewage sludge (Magdziarz et al., 2016), focusing on the prediction of solid and melt phases at feasible process temperatures.

The input data is the elemental composition of the combined feed, that is, fuel and air. This results on the most probable speciation of both vapor and condensed phases at a given temperature. One of the most valuable advantages of this comprehensive approach (Miller et al., 2002a,b) is the ability to process the chemical interactions among minor elements together with trace elements. The interpretation of trace metals partitioning is out of the scope of this work, although they have been included in the calculations, as shown later. Therefore, the discussion presented further down is limited to those minor ash-forming elements -like Na, K, Ca, Mg, Fe, Al, Si, Cl and P- that play a significant role in fly and bottom ash formation and whose species can be observed experimentally in the process ashes.

Since the potential relevance of irreversible phase segregation as the flue gas cools down is unknown a priori, two different calculation strategies were carried out. Fig. 1 shows a sketch of both schemes. The conventional approach (Fig. 1a) neglects the influence of the depletion of ash forming elements in the system, assumed as a closed one. The required input is just the elemental composition of the feed –system of both fuel and air loads- and a user-defined temperature range. Therefore, the availability of every element will be identical for each of the values in temperature series. A modified procedure, as sketched in Fig. 1b, was implemented to verify the potential rele-

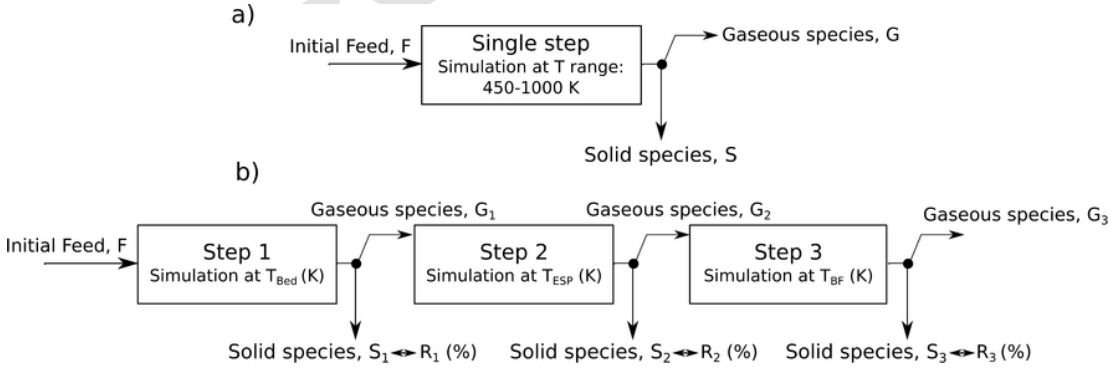

Fig. 1. Flowchart options for thermodynamic modeling. (a) Closed system and (b) Open system.

vance of irreversible phase segregation on the following simulation. In this case, assuming that the solid species formed leave the system, the material load at a given temperature is recalculated by subtracting the amount of condensed phase from the total mass of the system at the previous equilibrium calculation. A similar procedure has been described by Nutalapati et al. (2007) for the melt phase.

The driving hypothesis is that the availability of ash-forming elements can substantially decrease as flue gas cools down due to an irreversible gas-to-solid conversion. The solid species at the output (S_1) are considered to form the bed ash. The remaining gas species (G_1) are the input for the next step. The same procedure is followed for the other two process blocks, corresponding to the temperatures downstream of the heat exchanger and in the hybrid filter. Following this approach, the availability of each element decreases as simulated ashes are removed and the particular propensity to deplete in the gas phase is tracked by the parameter R_i. (Eq. (5)). It is defined as the molar ratio of the solid amount (S_i) generated at a given temperature to the total initial feed (F).

$$R_i = S_i(T)/F \tag{5}$$

In both approaches, the calculations were done at air-to-fuel ratios up to 45%, at atmospheric pressure and covering a temperature range of 450–1000 K. This range encompasses those of the main process blocks i.e. combustor bed, ESP and BF, where ashes are collected for validation purposes.

3. Experimental

3.1. Experimental set-up

The MCPs are, nowadays, one of the best available options for a sustainable management of waste biomass. The validation of these fuel engineering tools is based on the experimental data acquired in a 1 MWth (MCP according to the Directive (EU), 2015/2193, n.d.) located in a research facility (CEDER, Soria, Spain) and thus compatible with the deployment of a comprehensive experimental campaign. The combustor is a fluidized bed, firing industrial-grade pellets, able to operate in a multiproduct scheme. This plant can operate with up to three feeding lines for different biomasses or others solid fuels under a flow of 150–350 kg/h. The FB dimensions are 1 m in internal diameter and 4 m in height. It operates in bubbling regime, under an operation pressure slightly below atmospheric, fluidization velocity from 0.7 to 0.85 m/s, and the corresponding freeboard velocity from 1.4 to 1.55 m/s. The temperatures in the bed and freeboard are 720–750 °C and 830–860 °C respectively. Downstream of the heat exchanger, a Hybrid Filter (HF) allows an enhanced filtration and, thus, a control of fine particles as well as of the trace elements therein, while operating at high fractional efficiency levels in a multi-fuel scheme described elsewhere (Aragon et al., 2015). The HF consists of an electrostatic precipitator (ESP) and a bag filter (BF), serially connected. The BF provides 30 m^2 of filtering surface arranged in 8 rows of 24 pockets, and a back pulse cleaning system (Aragon et al., 2015). Flue gas flow rates were in the range of 1100–1250 Nm^3/h (d.b.), thus, within ±15%. In this experimental work, temperature in the HF ranges from 170 to 196 °C for fuel C, from 160 to 190 °C for blend BC, and up to 210 °C for blend AC, with a standard deviation of less than 20 °C throughout an operation day. The maximum applied voltage to ESP is 35 kV. In this experimental campaign, the applied voltage was set at 15 and 20 kV. The ESP and BF separated ash collection systems allow the off-line physicochemical characterization of the fly ashes along the hopper series. The experiments were performed along full shifts of stable operation indicated by the temperature immediately downstream of the heat exchanger (Aragon et al., 2015). FBs local hot spots showed lower temperature than ash fusion.

3.2. Compositional guidelines for blend design

Two blends using olive tree pruning waste as base fuel (Component C) were designed using waste materials of different inorganic composition to study the impact on ash behavior, while maintaining the equivalent thermal output of the plant. The main criteria for selecting the blend components were the relative concentration of some ash-forming elements along with the total amount of ash-forming matter in the fuel.

The addition of the component A, a composted fraction of sewage sludge, increases the Ca and P content in relation to fuel C, which should decrease the propensity to operational problems. It is widely accepted that displacing the K-conversion to yield compounds with a high melting point can solve the alkali problems during combustion (Li et al., 2013a,b). Karlsson et al. (2015) reported a significant decrease in corrosion co-firing sewage sludge with waste biomass (bark pellets) in a circulating FB.

The component B is a fraction of municipal solid waste with a high content on plastics. It has been selected due to its high Si content, which should lead to the formation of alkali silicates and, consequently, silica-melt related problems. Additionally, the admixture should fulfill other criteria related to the supply reliability and its seasonality.

The relatively high P content in component A should play an important role in the K reactions forming alkalis and alkaline earth phosphates with a high melting temperature such as $K_2CaP_2O_7$, K_3PO_4 and $KCaPO_4$, which would reduce the sintering propensity (Boström et al., 2009a; Ren and Li, 2015). The modification induced by the presence of P in the overall K behavior in co-combustion has been studied (Ren and Li, 2015) in a small-scale bubbling fluidized bed co-firing wheat straw with municipal sewage sludge, evidencing that P can react with K in both the fly ash and the bottom ash to form high melting T materials. Further evidence of the influence of ammonium phosphates on gaseous K release has been studied in a tube furnace- combustion of maize straw, cotton stalk and rice straw (Li et al., 2015). Boström et al. (2009a) used rapeseed meal rich in P, mixed with bark in a bubbling FB, concluding that the appropriate molar ratios PO_4^{3-}/K are between 1:1 and 2:1. In relation to the Ca role, Wang et al. (2011) remark that it presents the highest effectiveness in anti-slagging among the reactive ash-forming elements. However, calcium sulfate deposits are frequently observed on cold surfaces (Boström et al., 2012). Due to the low Si content, the presence of complex Ca silicates is not expected because these do not usually affect the chemistry of flue gases (Niu et al., 2016). The CaO path could lead to SO_2 production, and thus, increasing the yield of slag formation through alkali chlorides sulfation (Niu et al., 2016).

Component B contributes to a higher Si content boosting the probability of operational problems related to K-silica melt. Predictions of K release indicate a limitation at low K/Si ratio. For the fuel components used in this work, the K and Si concentrations will show a pattern of K > Si in the case of A, and Si > K in B. The K and Si concentration are higher in components A and B than the respective contents in base fuel C. However, the individual ratio K/Si, indicating the potential to enhance nucleation (Wiinikka et al., 2007) is higher in fuel C (2.01) than in A (1.77) and B components (0.30). Using the above-mentioned mixing ratios, the K/Si for blend AC (1.80) was

close to that for fuel C (2.01), showing the lowest value for blend BC (0.46), as it will be later discussed.

Chlorine is more abundant in both blends than in the base fuel. The chlorine-to-alkali molar ratio (Cl/(Na+K)) was 0.29, 0.40, and 0.09 for blends AC, BC and fuel C, respectively. This ratio warns against a higher trend of nucleation events, and consequently a higher corrosion ability of the raw gas. The Cl availability is the controlling factor for early inorganic aerosol formation in the absence of high sulfur content. As for the K/Na molar ratio, values were substantially different: 1.47 for blend AC, 0.91 for blend BC, and 11.29 for fuel C. Component A shows the maximum alkali content.

Compared with the mean values reported for woody biomasses (Vassilev et al., 2013b), the content of P as P_2O_5 in blend AC is largely out of range, and the S content as SO_3 although in the range is for all the fuels close to the upper limit. In contrast, the alkali content of all the fuels tends to be about or below the mean of typical woody biomasses. The SiO_2 content for all the blends is close to the minimum of the reported values (Vassilev et al., 2013b).

3.3. Fuel and ash characterization methods

The blends were characterized following European Standards (ASTM D-2361-95, 2001; EN 14774-2, 2009; EN 14775, 2009; EN 14918, 2009; EN 15104, 2011; EN 15148, 2009; EN 15289, 2011; EN 15290, 2011; UNE 32024, 1995) for calorific value, moisture content, ash, volatile matter, content of C, H, N, S, Cl, Al, Ca, Fe, Mg, P, K, Si, Ti and Na.

Ash characterization comprises chemical analysis as well as speciation of mineral phases. So far, operational prediction is usually based on analysis of ashes obtained by normalized procedures. Nevertheless, the ashing temperature varies among different standards: ASTM E870-82, (2013) employs 600 °C, ISO 540, (2008) employs 550 °C and GB/T 212, (2001) adopts 815 °C. Some authors, also, establish other values such as Thy et al., (2006) who use 525 °C. Xiao et al. (2011) recommend 600 °C from a purposely-designed study of the influence of ashing temperature on the resulting composition of some biomasses. Niu et al., (2013) discuss in detail the sudden and significant transformations in this range, mainly for K and Cl species. Since the ash is not a uniquely defined material, but strongly dependent on the combustion conditions, in this work both process and laboratory ashes have been analyzed to assess the implications of a given ashing procedure on the diagnosis derived from both kinds of fuel engineering tools.

The inorganic matter (Al, Ca, Fe, K, Mg, Na, P, S, Si, Ba, Mn, Sr, Ti and Zn) has been analyzed following the standard EN 15290 (2011). Laboratory ashes obtained at 550 °C from "as received" materials were digested in a microwave oven and then analyzed by ICP/AES using a THERMO JARRELL ASH spectrometer. Process ashes were analyzed using ICP/MS (Na, K, Ca, Mg, Cl, S, Si, Al and P) and ICP/AES (Na, K and S) model Varian 735ES, and XRF (Na, K, Ca, Mg, Si, Al, P, and Fe) model PANalytical Axios.

Mineralogical identification has been carried out by means of powder X-Ray diffraction (XRD) using a PANalytical Xpert PRO diffractometer with Cu K_α radiation ($\lambda = 1.5418$ Å), with generator set at 40 KV and 40 mA, and diffractograms recorded in the 5–80° 2theta range. The relative proportions of the phases have been obtained by applying Reference Intensity Ratios (Hubbard and Snyder, 1988) values to the area of the strongest peaks for each phase, to reduce the effect of overlapping found in complex experimental diffraction patterns.

4. Results

Experimental results as well as predictions are shown below. First, the fuel blend characteristics and their implications are discussed; then, the observations on experimental ashes and finally, the operational diagnosis derived from the above mentioned prediction tools.

4.1. Fuel characterization

Base fuel C is olive tree pruning waste, component A is a composted fraction of sewage sludge and component B is a fraction of municipal solid waste with a high content on plastics. Mixing ratios in the blends AC and BC were 50/50 (%wt) approximately, under a constraint of a high heating value (HHV) around 20 MJ/kg, whatever components are present.

The blend components have been pelletized separately, and upgraded through the exclusion of any extraneous inorganic matter, which could be added during harvesting, handling and processing of the material. Due to the proper storage conditions, the humidity of the three components is relatively similar and shows lower values than the raw resource.

The differences in Ash, FC, N and S content of fuel C, when are compared with literature data, for instance those reported in García et al. (2012) for olive tree pruning, can be ascribed to regional differences in fertilizing, harvesting, storage and pretreatment procedures. The parameters more closely related to the vegetal structure, such as HHV, VM, RH, C, H and O exhibit much less variability.

Table 1 summarizes the composition and heating values of the three components (A, B, C) and the blends (AC, BC), calculated using the actual mixing ratio using a linear superposition approach. The proximate analysis presents differences among the ash content, VM and FC among the fuel C and their blends. Especially relevant for operational purposes are those related to ash content. For instance the blend AC contains 300% of ash in comparison to fuel C, which in

Table 1
Heating values (MJ/kg) and composition (wt%) of blends and their components [4].

	Compost (A)	MSW (B)	Olive prune (C)	Blend AC (49:51)	Blend BC (45:55)
	Heating values (MJ/kg)				
HHV	16.62	24.04	19.12	17.89	21.33
LHV	15.48	22.53	17.78	16.65	19.92
	Relative humidity (%wt. w.b.)				
RH	10.15	8.80	7.47	8.78	8.07
	Proximate analysis (%wt. d.b.)				
Ash	25.30	21.10	5.07	14.98	12.28
VM	64.80	75.50	81.27	73.20	78.67
FC[a]	9.90	3.40	13.67	11.82	9.05
	Ultimate analysis (%wt. d.b.)				
C	38.85	51.70	47.43	43.23	49.35
H	5.25	7.00	6.17	5.72	6.54
O (diff)	23.36	17.92	40.49	32.09	30.33
N	5.77	1.24	0.74	3.20	0.96
S	0.58	0.28	0.08	0.33	0.17
Cl	0.90	0.76	0.03	0.45	0.36
	Elemental analysis (%wt. d.b.)				
P	0.353	0.027	0.007	0.177	0.016
Si	0.097	0.207	0.018	0.056	0.103
K	0.171	0.061	0.035	0.102	0.047
Na	0.082	0.066	0.002	0.041	0.031
Ca	0.732	0.347	0.161	0.441	0.244
Mg	0.072	0.022	0.014	0.043	0.018
Al	0.009	0.156	0.004	0.007	0.073
Fe	0.006	0.066	0.002	0.004	0.031

turn implies operational challenges for both deposit prevention and atmospheric emissions. The concentration of volatile matter (81.27% d.b.) in fuel C is the highest, although the blends present values near to 75%wt. The fixed carbon concentration (FC) in fuel C is the highest, although the three values are within the range of 9–12%. Blend BC shows the highest values and the lowest for elemental C and for FC, respectively.

In order to compare the energetic and chemical behavior of these fuels with other biomasses, some widely used diagrams are adopted from the literature. Fig. 2 shows the Van Krevelen diagram relating the H:C and O:C atomic ratios for different fuel categories, which are associated to areas of similar characteristics and properties, such as the calorific value. Generally, biomass fuels present higher ratios than coal (1.2–1.8 in H:C and 0.4–0.8 in O:C). The fuels used in this study have approximately the same H:C ratio (1.6), although they differ in the O:C ratio (0.25–0.65). Component C, the most oxygenated one, lies in the middle of the biomass area as defined by Jenkins et al. (1998). Component A falls in the lower limit and component B is located outside this area. In spite of that, both AC and BC blends can be considered as biomass according to their energetic potential (Jenkins et al., 1998).

Fig. 3 presents two ternary diagrams from the fuel proximate and ultimate analysis as defined by Vassilev et al. (2015). The first one represents the biomass area using VM, FC and ash content, whereas the second displays the classification of both the components and blends according to the C+H, O and N+S+Cl content. Fuel C is located near to wood and woody biomass positions, blends AC and BC show a close match to the herbaceous biomasses and contaminated biomass group, respectively. Thus, according to these ternary plots and in agreement with Van Krevelen diagram, fuel C and its blends can be considered as biomass or biomass-like fuels.

The absolute content and the atomic ratios of most important ash forming elements with respect to raw aerosol formation and further condensed phase reactions (Boström et al., 2012) are shown in Fig. 4. The discussion about ash fusion propensity must be based not only on the chemical composition but also on the presence of refractory versus fluxing minerals, as will be discussed later on, retrieving the information from ash characterization. The S and Cl content ranges from 0.08 to 0.33% wt. d.b., and 0.03 to 0.45% wt. d.b., respectively. In both cases, the lower values correspond to fuel C and the highest to blend AC. However, the ratios of S and Cl to total alkalis highlight differences in the S and Cl related chemistry; whereas the values of Cl/(Na+K) follow a clear tendency (fuel C < blend AC < blend BC), S/(Na+K) is practically similar for all the fuels.

The blends show a priori different tendencies in elements attributed to pro- and anti-slagging contributions. Whereas BC shows the highest content in Si and Al, blend AC has the highest content of Ca, P, S and alkalis. Fuel C presents the lowest content in Fe, Na and P.

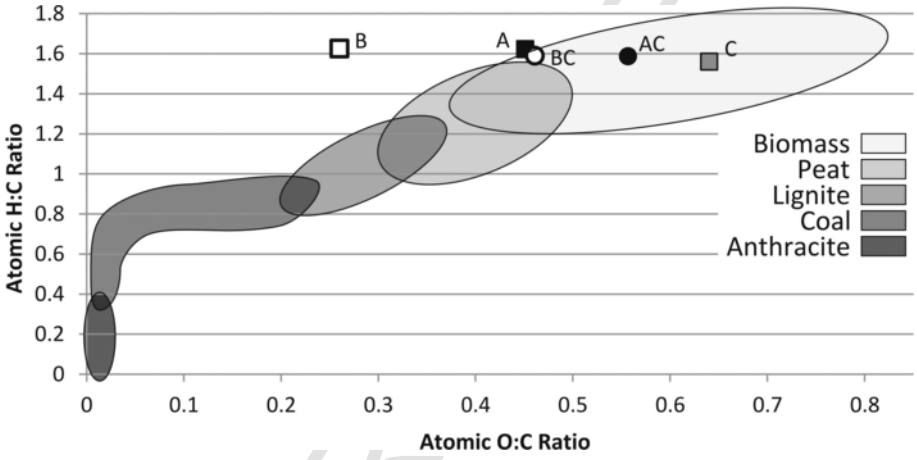

Fig. 2. Position in the Van Krevelen diagram, adapted from Jenkins et al. (1998), of the fuel, components and blends and the general loci of coal and biomass fuels.

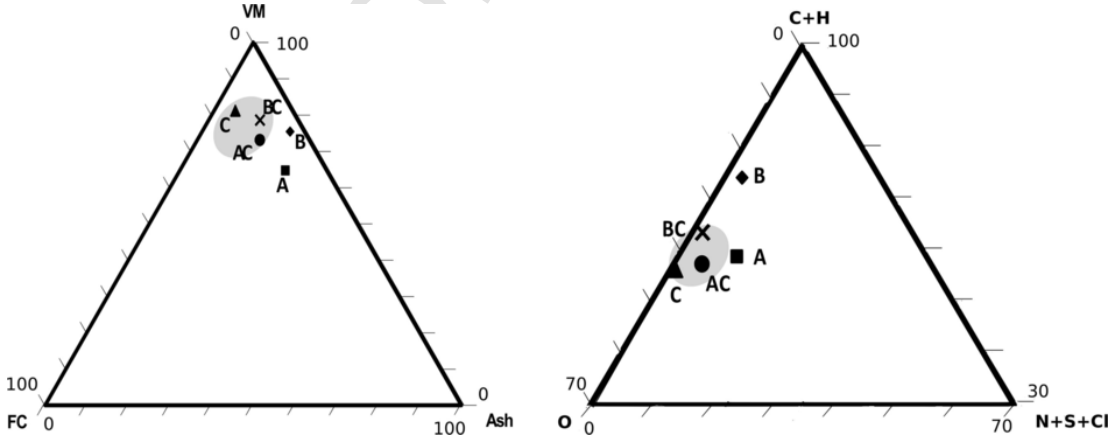

Fig. 3. Compositional (wt%) positions of the blends relative to the area attributed to biomass (grey) (Vassilev et al., 2015). (For interpretation of the references to colour in this figure legend, the reader is referred to the web version of this article.)

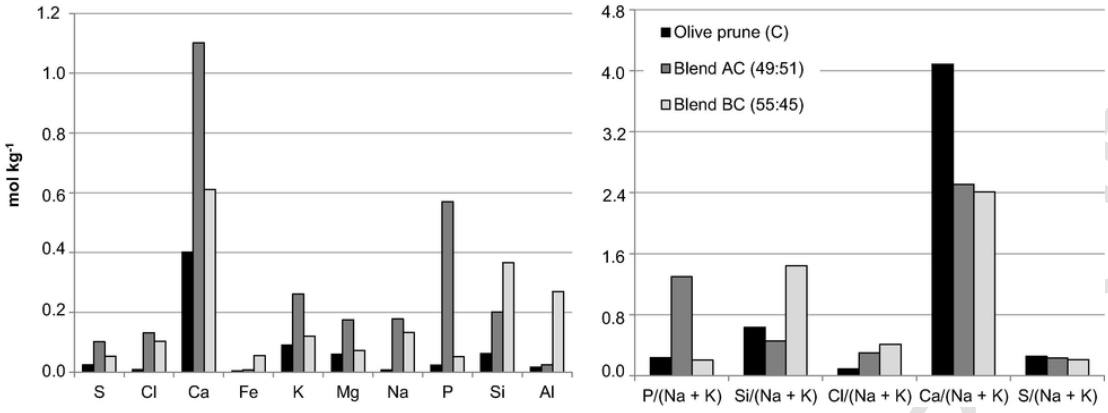

Fig. 4. Atomic content (a) and ratios (b) of ash-forming elements in the fuel and its blends.

The ratio of P to total alkalis of blend AC is about four times the corresponding values for blend BC and fuel C. The ratio of Si to total alkalis of blend C reaches up to three times the values for both blend AC and fuel C. The Si content in blend BC is slightly greater than five-times the corresponding value in fuel C; the Ca content in blend AC is around 2.5 times the corresponding value in Fuel C. However, the highest Al content is present in blend BC; about 7.5 times of that of fuel C.

4.2. Ash characterization

The results for both laboratory (550 °C) and process ashes are presented as follows: major ash elements as oxides and its position in compositional maps qualifying their propensity to operational problems, elemental analysis of the process ashes and crystalline phase composition (XRD) of bottom ashes from the ESP and the BF.

The composition, as conventionally expressed as oxides, is shown in Table 2 together with typical values (Vassilev et al., 2013a) for woody biomass for the sake of comparison. These concentrations span over a quite wide range, as is reported. Values in Table 2 are reported for both the laboratory ashes (550 °C) and the material collected at the MCP, thus having undergone the corresponding transformations at the temporal evolution of temperature along the process line. As a general trend, standard ashing leads to an underestimation of the oxide content with the exception of CaO and SiO_2. These differences range up to about 50% in the case of SO_3 as observed by Magdziarz et al. (2016). However, the composition of blend BC ashes shows an opposite tendency, since standard ashing overestimates the content in K_2O, contrary to the general behavior as in Xiao et al. (2011) indicate, it while underestimates the SiO_2.

The concentration as oxides in both ashes (laboratory and process) falls close to the mean value reported by Vassilev et al. (2013a). In the case of laboratory ashes, the CaO concentration of fuel C is 59.60% compared to the average of 43.03% and the AC blend presented 19.41% of P_2O_5 compared to the mean value of 3.48%. The process ashes result in analogous compositional pattern as the laboratory ones. The CaO content in fuel C is 48.76% and the P_2O_5 content is 20.5% in blend AC. Both ash points– at the process and at the so-called standard temperatures- are displayed in Fig. 5 on the ternary diagrams proposed by Vassilev et al. (2014) to link the ash composition expressed as oxides and the potential operational problems.

The chemical and mineral characteristics of the ashes collected along the HF are discussed below. The itemized elemental profiles of process ashes are shown in Fig. 6. A clearly distinct profile is observed, depending on the fuel for ESP and BF ashes, thus reflecting the size distribution of the chemical signature. Ashes from the ESP hoppers are more concentrated in Ca, P and Si, to a larger extent in the blends than in fuel C, while ashes collected by the BF are relatively enriched in Na, K, Cl and S. The influence of blending on al-

Table 2
Chemical composition (wt%) of the ashes at different ashing temperatures and compared with literature data for woody biomass (Vassilev et al., 2013b).

	SiO_2	CaO	K_2O	P_2O_5	Al_2O_3	MgO	Fe_2O_3	SO_3	Na_2O
(a) Laboratory ashes at 550 °C									
Fuel C	9.99	59.60	11.29	4.39	2.24	6.36	0.87	4.48	0.67
Blend AC	8.74	47.51	9.26	19.41	1.32	5.28	0.56	5.22	2.67
Blend BC	17.62	45.21	8.06	4.04	9.39	4.38	3.10	4.32	2.82
(b) Process ashes at FB temperature (900–1000 K)									
Fuel C	5.85	48.76	15.25	6.70	3.88	7.93	1.47	8.32	1.84
Blend AC	7.94	37.26	13.11	20.15	2.05	4.54	1.14	9.56	4.25
Blend BC	18.03	35.25	7.31	5.39	15.58	3.87	4.08	6.03	4.46
(c) Typical ashes for woody biomass									
Mean	22.22	43.03	10.75	3.48	5.09	6.07	3.44	2.78	2.85
Min	1.86	5.79	2.19	0.66	0.12	1.10	0.37	0.36	0.22
Max	68.18	83.46	31.99	13.01	15.12	14.57	9.54	11.66	29.82

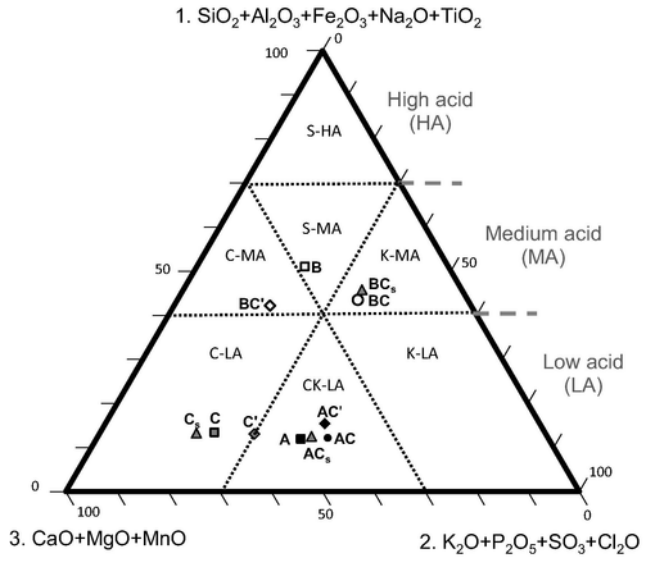

Fig. 5. Compositional plot, adapted from Vassilev et al. (2014) of laboratory (550 °C), process and predicted ashes, expressed as oxides (wt%).

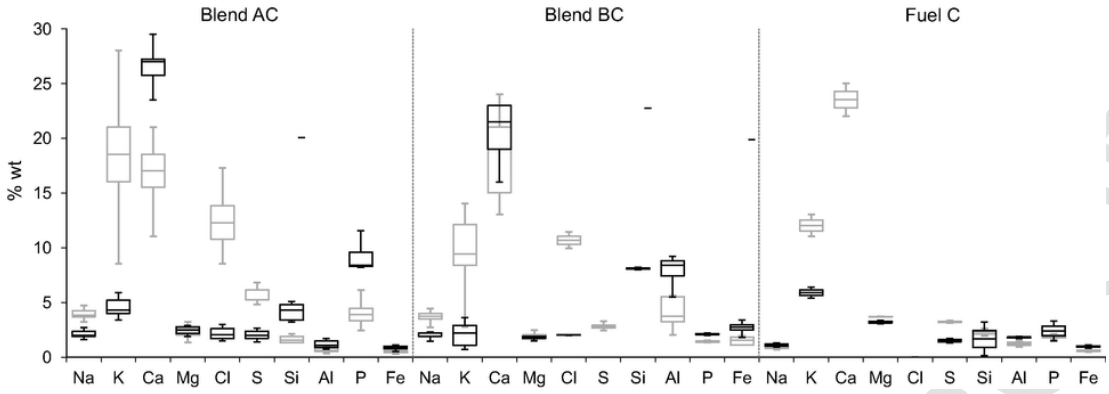

Fig. 6. Chemical profiles for ashes along the flue gas line for ash-forming elements (%wt. d.b.) Black (ESP). Grey (BF).

kali concentration is basically attributed to K, and shows a substantial contribution in the case of blend AC.

The ESP and BF ashes were analyzed by XRD. Fig. 7 shows an example of a typical diffraction pattern, which reflects the complexity of the mineral composition as well as the presence of a minor although non-solved amorphous matter. The major reference peaks–whose situation is signaled by vertical lines-, are observed and further assigned to specific species. XRD data processing is encapsulated in Fig. 8.The most abundant mineral phases are in agreement to those itemized in Boström et al. (2012) with the exception of halite and gehlenite. A number of phases reported such as feldspars, periclase, magnetite and several alkaline earth silicates among others (Boström et al., 2012) have not been identified in this study. The more abundant species in fuel C ash are calcite, apatite and portlandite, in both ESP and BF hoppers. K is present in form of arcanite and sylvite, both species clearly biased towards the BF ash. Blend AC presents a higher abundance of apatite as the major P-containing phase in the ESP than in the BF ashes. Alkali-containing phases are mainly aphthitalite and a smaller quantity of sylvite, the latter being strongly displaced to the BF ash, which also shows the presence of halite about 5%. The identified silicate minerals are quartz and merwinite (a double sulfate of alkaline earth elements) in minor amounts in the ESP ash. The pattern of most relevant phases in blend BC ashes is noticeably different. The Ca-containing phases account for about 85% in the ESP whereas in the BF about 50%. The alkali-containing phases (sylvite, aphthitalite) account for about 10% of the mineral content in the ESP ash, but this value increases up to 50% in the BF, confirming the tendency to form fine particles. K_2SO_4 is present only in the fuel C, although K,Na-sulfate appears in the blends, always displaced to the BF ashes. The low presence of alkaline chlorides indicates their presence in the flue gases.

4.3. Diagnostic based on ash composition

This type of diagnosis is about customarily elemental composition expressed in the form of oxides.

Table 3 encapsulates the diagnosis obtained from a suite of criterion numbers based on the oxide composition of the standard ashes. The three $R_{B/A}$ numbers indicate all that severe ash-related problems should be expected firing these fuels. This ratio shows extremely high values for fuel C and blend AC, and a lower index for BC, although in all the cases these values are sufficiently higher than the in-

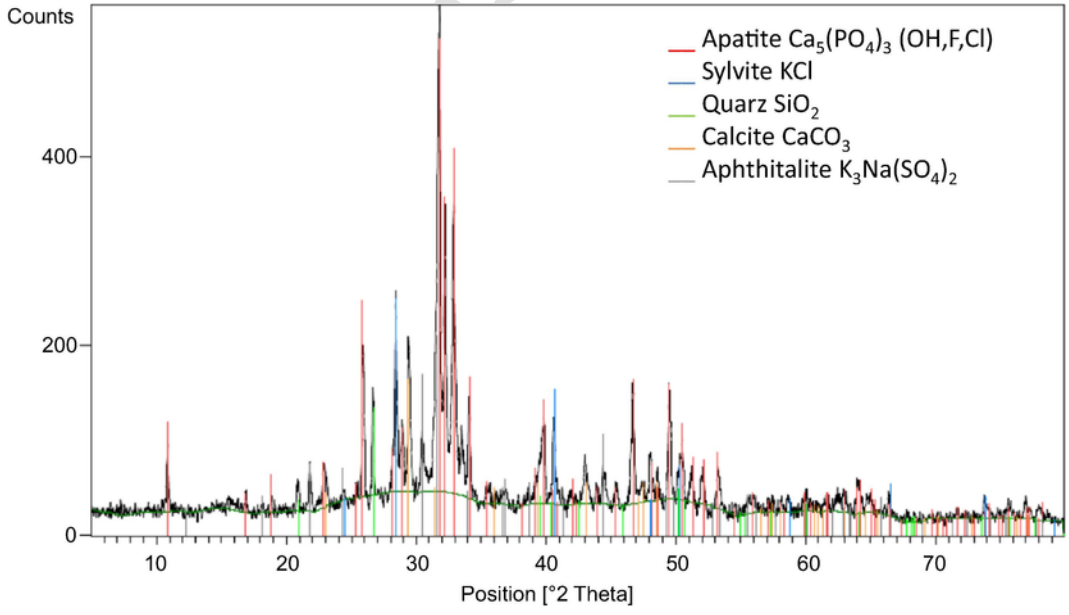

Fig. 7. Diffraction pattern of ESP ashes firing Blend AC.

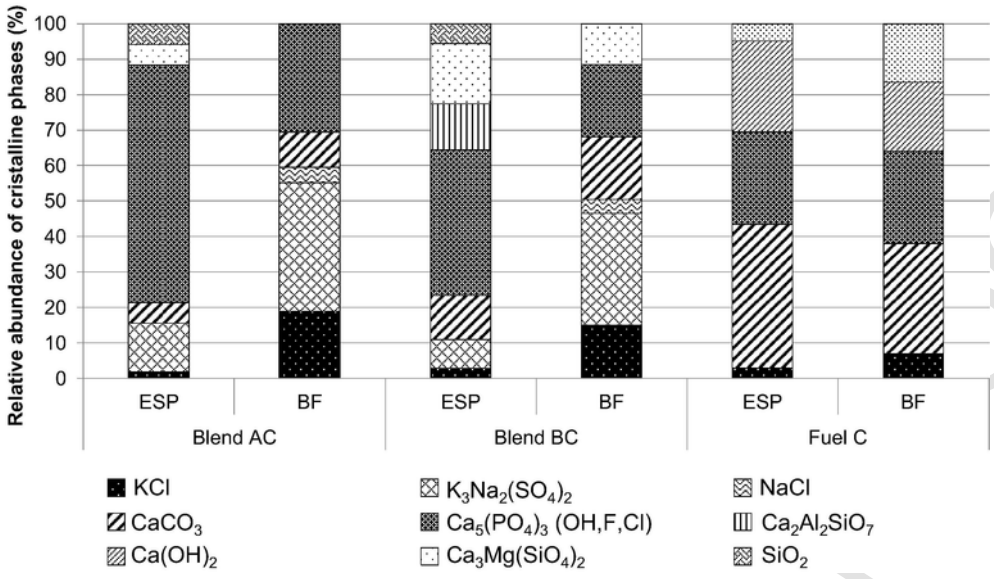

Fig. 8. Relative abundance of crystalline phases in ESP and BF ashes firing Fuel C and its Blends. Nomenclature: KCl (sylvite), $Ca_2Al_2SiO_7$ (gehlenite), $K_3Na(SO_4)_2$ (aphthitalite), $Ca(OH)_2$ (portlandite), NaCl (halite), $Ca_3Mg(SiO_4)_2$ (merwinite), $CaCO_3$ (calcite), SiO_2 (quartz), $Ca_5(PO_4)_3$ (OH, F, Cl) (apatite), K_2SO_4 (arcanite).

Table 3
Diagnostic of slagging and fouling propensity based on criterion numbers.

Index	Fuel C	Blend AC	Blend BC	Ref	Diagnostic		
					Fuel C	Blend AC	Blend BC
$R_{B/A}$	6.39	6.46	2.26	Vassilev et al, 2013	⇧⇧	⇧⇧	⇧⇧
$R_{B/A(+P)}$	6.75	8.38	2.41	Teixeira et al., 2012			
$R_{B/Asimp}$	5.46	5.30	1.95	Jenkins et al., 1998			
S_R	13.00	14.08	25.06	Teixeira et al., 2012	⇧⇧	⇧⇧	⇧⇧
Cl ratio	1.03	1.48	0.51	Pronobis, 2006	⇧⇧	⇧⇧	⇩
S ratio	1.12	1.39	0.47				
Fu	76.43	77.11	24.65	Jenkins et al., 1998	⇧⇧	⇧⇧	⇧

⇧⇧ Severe slagging and fouling probability.
⇧ High slagging and fouling probability.
⇩ Low slagging and fouling probability.

dicator of high propensity. However, no selective blending guidance can be obtained for this kind of prediction. The same can be concluded from modified $R_{B/A}$ numbers; in particular, $R_{B/(A+P)}$ does not present significant advantages over $R_{B/A}$. The Cl and S ratios indicate severe slagging propensity for C and AC, whereas this tendency is low for blend BC in contrast to the predictions using $R_{B/A}$ numbers. In this case, the S ratio has been calculated taking the total S content in the biomass, as S volatile, thus, considering that the full S content is oxidized to SO_2. As total S will be always higher or equal to volatile S, the resulting values are overestimations of the S ratio. This approach is a conservative one and does not entail any detectable gross error in the final diagnosis from S ratio index.

In Fig. 5, process and laboratory ash composition are located on the ternary diagrams proposed by Vassilev et al. (2014) to link the ash composition and the potential operational problems. Process ashes are denoted as C′, AC′ and BC′ and the standard ones as C, AC, BC, respectively. The boundaries of the regions represented (Vassilev et al., 2014), assign to biomass fuels with lower alkali, Cl, Si and ash, and with higher Ca contents a more manageable behavior. ‘‘C-MA’’ and ‘‘C-LA’’ should represent the best positions to prevent fouling and slagging.

The blend ashes can be classified in substantially different regions than those of the original components, as is the case for B but not for A. For instance, component B position within the S-MA anticipates probable slagging and fouling. In general, component B leads to positions in the medium acid region and component A in the low acid region. Point C lies within the ‘‘C-LA’’ sub-type, which includes almost entirely woody biomasses but C′ moves to the boundary between C-LA and CK-LA types. The ‘‘CK-LA’’ sub-type gathers biomass ashes of low acid tendency such as those from component A. Both AC and AC′ points lie within the same region, thus the operational diagnosis will not be sensitive to the ashing temperature.

BC but not BC′, is located within “K-MA” region, which represents the worst conditions, that is, ashes with lower fusion temperatures, short softening–melting range and high flow-dissolution rate. Thus, the estimation from standard ashing leads in this case to a more severe prognostic that can even hinder the use of this blend.

4.4. Diagnostic based on thermodynamic equilibrium

Given that the relevance of the condensed mass fraction at a given temperature is a priori unknown; two different calculation procedures have been adopted, as above discussed. Table 4 encapsulates the molar percent (in relation to the total amount of solids) for the major species, based on both a closed and an open system approach. As previously defined, the closed system approach neglects the irreversible segregation of the condensed phase; thus keeping constant the availability of each element for the formation of species along a wide temperature range. In the case of the open system approach, the simulation proceeds step by step and the system mass and composition is recalculated assuming that the solid phase formed at a given temperature is completely separated. The temperature ranges are between those reached in the HF (400–500 K) and the maximum in FB (900–1000 K). Here are presented the results for an initial elemental load calculated for a 45% of excess air, close to the operation conditions.

Table 4
Molar percent share of main species to the total amount of solid phase along the gas line, and relative amount of solid formation in the case of open systems.

				Open System			Closed System		
				C	AC	BC	C	AC	BC
Species				Fluid Bed (975–990 K)			Fluid Bed (950 K)		
Ca	P		$Ca_3(PO_4)_2$	1.6%	39.3%	5.1%	1.6%	38.5%	*
			$CaCO_3$	72.5%			72.3%		*
			$CaFe_2O_4$	0.5%	0.5%	6.3%	0.5%	0.5%	*
	Si		Ca_2SiO_4			7.3%			*
			$Ca_2Al_2SiO_7$			23.1%			*
		Mg	$Ca_3Mg(SiO_4)_2$	7.9%	5.3%	16.5%	7.9%	5.2%	*
			$CaMgSiO_4$		17.0%			16.8%	*
			MgO	5.3%	0.9%		5.3%	0.1%	*
K	Cl		KCl		14.4%		0.6%	16.5%	*
	S		K_2SO_4	6.3%	9.6%	0.6%	6.3%	9.0%	*
Na			Na_2SO_4		4.6%	11.4%		4.6%	*
			Na_2CO_3	0.9%	7.3%		0.90%	7.3%	*
			R_i	0.14%	0.28%	0.15%			
				ESP (450–482 K)			**ESP (500 K)**		
K	Cl		KCl	88.4%	59.8%	76.3%	1.8%	6.5%	11.2%
Na			NaCl	10.6%	17.5%	22.3%		8.0%	1.3%
			Al_2O_3		22.3%				
Ca			$CaCO_3$				81.1%	25.8%	61.1%
	P		$Ca_3(PO_4)_2$				1.6%	32.3%	3.2%
			R_i	< 0.01%	0.01%	0.01%			
				BF (445–475 K)			**BF (450 K)**		
			SnO_2	100%					
			TlCl		100%	100%			
Ca			$CaCO_3$				73.8%	19.4%	61.1%
	P		$Ca_3(PO_4)_2$				2.5%	33.4%	3.2%
K	Cl		KCl				1.8%	6.8%	11.2%
	S		K_2SO_4				5.4%	11.8%	1.8%
			R_i	<0.01%	<0.01%	<0.01%			

Table 4-left- shows the results following the open-system approach, including the major species and the elemental solid fraction (R_i) produced at each temperature. It is observed that the higher R_i values correspond to the highest temperature, although the absolute value is as low as 0.28% mole basis. Therefore, in this particular case no substantial implications on the final bottom and fly ash major species are to be expected. At lower temperatures such as those prevailing in the HF, R_i takes a value of about 0.01% mole basis, where the predominant species are alkali chlorides (KCl and NaCl), presumably present in the fine particles.

Finally, Fig. 9 presents the closure of the elemental composition obtained from thermodynamic equilibrium against the analysis of process ashes.

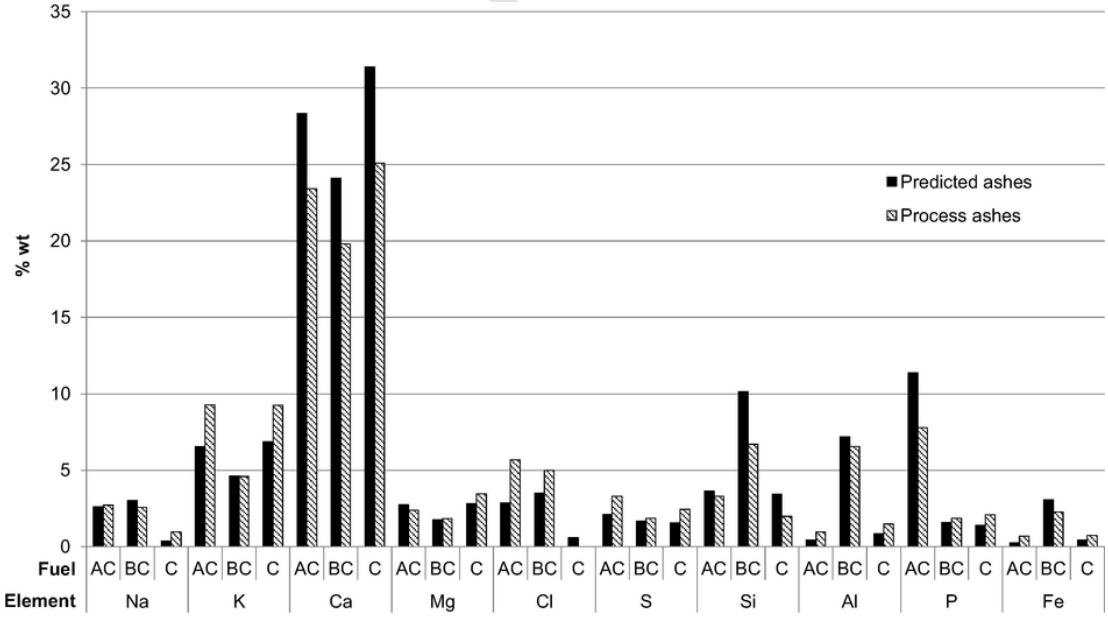

Fig. 9. Elemental closure between thermodynamic prediction (striped columns) and elemental analysis of process ashes (solid columns).

It is observed how the prediction overestimates Ca and Si content in ash, and in contrast, underestimates K, S and Cl content. Nevertheless, these differences never exceed a 5% wt.

It is important to recall that a systematic bias is to be expected, which will result in higher values from prediction. This is due to the fact that whereas equilibrium modeling gives a total amount of each chemical, irrespective of the stream, the experimental analysis has been conducted merely on the solid process stream. Consequently, this bias is expected to be more important for those compounds whose partition is more pronounced to the aerosol.

The simulation results of the solids are also integrated in the phase diagram in Fig. 5. The compositions of these predicted "ashes" are represented as C_s, AC_s and CB_s in the diagram.

5. Discussion

As above mentioned, the olive tree pruning waste-based blends have been designed to show extreme and opposite behavior, although keeping roughly constant the thermal output. Some noticeable differences in ash content are present between the olive tree pruning and their blends. The ash content in blend AC is three times higher than the fuel C content and 2.5 in the case of blend BC. The slag formation properties are affected by both total ash content and chemical composition. Component A contributes noticeably to the K content, which should indicate a higher propensity to alkali-induced corrosion in the absence of S, due to KCl deposits. However, the mere consideration of K content is not sufficient for a prediction of the behavior of AC ashes. In the case of a significant S content, as in blend AC, sulfation will take place at high temperature, decreasing the K availability for chlorine-based deposits. Component B contributes to the Si and Al content, which increases the formation of alkali silicates and, consequently, silica-melt related problems. Therefore, the blends will be more problematic than the base fuel C.

The chemical fingerprint of fly ash as well as the mineral phases of the material collected along the HF, show that the alkali content firing AC, and in less proportion firing BC, is higher and exhibit a greater variability than fuel C ashes (Fig. 6). From Fig. 8 it can be observed how the abundance of alkali minerals in the ESP ashes firing blend AC accounts just for 15%, whereas in the BF ashes this value rises up to 60%. It can be observed that Ca is the most abundant component and competes in the formation of phosphate and sulfate. However, due to the higher available P content, calcium forms mainly Ca-phosphate, while sulfur is available to the alkaline sulfate formation. The same occurs firing blend BC, the abundance of alkali minerals in the ESP ashes is about 12% whereas in the BF ashes it increases to 51%.

The differences of elemental composition between the BF and the ESP ash, even for a given fuel reflect the ability of some elements to concentrate in the size bins penetrating the ESP. A detailed discussion of the aerosol characterization downstream the HF can be found in Aragon et al. (2015). The particles whose size fall within the ESP penetration window (>0.5 μm range) are enriched mainly in Na, K, Cl and S, whereas the ashes from the ESP hoppers are more concentrated in Ca, P and Si, to a larger extent in the blends, as observed in Fig. 6. Alkaline earth minerals are more abundant in ESP ashes, and a shift to the BF is observed for the alkaline phases related to the ESP penetration window. Fig. 7 shows how the BF ashes are in all the cases enriched in KCl, $K_3Na(SO_4)_2$, NaCl, and K_2SO_4; while ESP ashes are more concentrated in $Ca_5(PO_4)_3$, $Ca_2Al_2SiO_7$, $Ca(OH)_2$, $Ca_3Mg(SiO_4)_2$). A noticeable difference between fuel C and blend is that in the former case the differences between ESP and BF ashes are less pronounced.

Hereinafter, the results using the two types of approaches will be shown and their match to both experimental results and literature data is discussed. The ability of the diagnosis tools in providing blending criteria is determined from a congruence assessment and also from a comparison with experimental data.

As Fig. 5 shows, the influence of ashing temperature on the diagnosis from ternary diagrams cannot be generally ignored. In the case of blend AC, little difference is observed between AC′ and AC positions in the "CK-LA" area. This is not the case for blend BC, whose ashes can fall within different regions, depending on the temperature, leading to contradictory predictions. At standard ashing temperature (550 °C), blend BC is classified in the ''K-MA'' sub-type, usually associated to herbaceous and agricultural biomass and rarely from woody biomasses (Vassilev et al., 2014). The ''K'' type should show, according to the literature (Vassilev et al., 2014), comparatively high values of K, S and Na, which is not consistent with the elemental composition as shown in Fig. 4. At process temperature, BC ashes position moves to C-MA area, leading to a completely different a priori description of the ash behavior that is from the worst case of slagging to a moderate one. This highlights the importance of a realistic assay temperature and suggests the appropriateness of a harmonization of the prediction tools and the conditions of ash generation in real life.

The diagnostic suitability of criterion numbers is also significantly dependent on the ashing temperature, as in Xiao et al. (2011). The results display a low sensitivity of the diagnosis to the fuel, allocating similar numbers to very different ashes, although it is claimed they provide qualitative guidance on the propensity of the ashes to trigger operational problems. Moreover, some disagreement with the information from the phase diagrams is observed. According to the phase diagrams, blend BC presented the highest propensity to operational problems, whereas, according to the criterion numbers in Table 3, it presents a lower slagging and fouling propensity, obtaining lower values than blend AC and fuel C.

The diagnosis from thermodynamic prediction is compared with the mineral ash composition in order to validate the scope of this kind of tools. Due to the similarity of both simulation strategies at high temperatures, the species and phases predicted were, as expected, very similar with the exception of $CaCO_3$ firing BC. The differences arise when cooling down the flue gas, due to irreversible phase segregation. As it is observed in Table 4, firing fuel C, the prediction of main species in the ash ($CaCO_3$, $Ca_5(PO_4)_3$, $Ca(OH)_2$, K_2SO_4 and KCl) matches the XRD observations. In the case of P species, the difference between the prediction as $Ca_3(PO_4)_2$ and the observed apatite could be attributed to further recombination in the ash, due to the temperature and vapor pressure (Boström et al., 2012). At low temperatures (450–500 K), the amount of K_2SO_4 and KCl increases in comparison with the obtained at high temperatures. In case of the blends, the amount of KCl and K_2SO_4 also is higher at low temperatures. These potassium species are present also in XRD results, increasing along the HF (higher concentration in BF than ESP). For blend AC, the main phases at high temperatures are in agreement with XRD results, except $CaCO_3$ (present at low temperatures): Na_2CO_3 and $CaMgSiO_4$ which are not observed by XRD. Furthermore, alkali sulfates appear as Na_2SO_4 and K_2SO_4 in thermodynamic simulation, while in XRD they appear as $K_2Na(SO_4)_2$. Again, at low temperatures, new species appear whose real contribution is not detected by XRD. For blend BC, several Si species are predicted, mainly $Ca_2Al_2SiO_7$ and $Ca_3Mg(SiO_4)_2$, which are also observed by XRD. The main mineral phases observed by XRD, with the exception of apatite and aphthitalite, are predicted by MTDATA, which in turn

identifies $Ca_3(PO_4)_2$ as the most probable species of P without any combination with individual alkali sulfates.

Therefore, several differences are observed: (1) some compounds are not identified by XRD, mainly those containing Mg, Si and Al. In the case of fuel C, $Ca_3Mg(SiO_4)_2$, MgO, K_3PO_4 and $MgAlO_4$ are identified; firing AC,$CaMgSiO_4$, Na_2CO_3 and Al_2O_3 and for BC,Ca_2SiO_4, $CaFe_2O_4$, $Na_2Al_2Si_6O_{16}$ and other minor phases. (2) Chemical equilibrium does neither predict the formation of a double alkaline sulfate ($K_3Na(SO_4)_2$) - yielding instead in single sulfates- nor the formation of apatite ($Ca_5(PO_4)_3$) and portlandite ($Ca(OH)_2$). This fairly agree with the mineral phases identified for a suite of biomasses by Vassilev et al. (2013b) within a wide range of temperature. The main discrepancies arise at low temperatures, and correspond to the presence of feldspar and sodium carbonates, which are not detected, at least above the detection limit, in this work. The more pronounced abundance of silicates in this work is attributed to a higher Si-content in the blends used in these trials, because of equilibrium predictions ranging from 5 to 17% merwinite and, for example up to a 23.1% of calcium aluminosilicate firing BC. The higher content of silicates in the blend BC would indicate the greater probability of formation of a melting phase, which would trigger the deposits formation on the internals. Blend AC presents a smaller number of silicates, so less propensity to these operational problems.

In Fig. 5, it can be observed how the predicted ashes are located in very close positions with respect to the real ones, validating the thermodynamic prediction. Therefore, it will be possible to predict the suitable position for the combustion, based on the biomass composition, excess air, combustion temperature, the composition of the solids generated, and by using the triangular diagram.

6. Conclusions

The usefulness of prediction tools can be crucial for MCP firing agricultural or forestry wastes due to the intrinsic seasonality in supply and, thus, the feasibility of blending.

Fuel engineering provides guidance on the blending criteria for both prevention and mitigation of ash related issues in waste biomass combustion. Two types of prediction methods have been used: using the composition of ash and using the fuel/air ratio to be fed to the boiler. However, the predictions based on the ash composition can be strongly dependent on the ashing temperature. The use of criterion numbers needs a previous assessment of the similarities between the target biomass and the empirical basis of these ranking indexes. Predictive tools, diagrams and criterion numbers, can result in different diagnoses for the same blend. For instance, blend BC presents, using the triangular diagrams, the highest propensity to operational problems, while the criterion numbers indicate lower values than blend AC and fuel C. In the case of the thermodynamic prediction for this blend, similar results have been obtained to those from triangular diagrams.

As an alternative for prediction, multiphase equilibrium modeling does not require any additional information or assumption on ashing procedure (temperature and equivalence ratio); therefore, it is an effective way to avoid the information loss associated to the volatile species in the range of temperature from ashing to process conditions. The elemental closure for the main ash-forming elements was above 95%. Since the fluidized bed operates in the bubbling regime, the thermodynamic system can be assumed as a closed one without a noticeable loss in accuracy of prediction.

Although the prediction through equilibrium calculations does not pretend to give an operational diagnosis, it opens the possibility of assessing the ash sensitivity to both blend formulation and equivalence ratio. Moreover, this sensitivity study can be done in an a priori way, thus enabling an effective method for operational problems prevention.

The validation of predictive tools has been carried out at MCP scale, firing pellets based on olive tree pruning waste and its typical blends. A separated characterization of ESP versus BF ashes reflects the size-distributed chemical composition. The sub-micrometer particulate matter in the flue gas of woody biomass combustion mainly consists of alkali sulfates and chlorides (as observed by XRD and thermodynamic prediction). The crystalline phase proportions reflect the composition of the fuel concerning K, Cl, and S, with respect paid to bottom ash temperature conditions and K retention properties in the form of reactive Si. Although its relevance is critical for the HF performance, it is not the case for ash-related prevention purposes.

Chemical equilibrium simulations obviously differ from real ashes due to the influence of a suite of rate phenomena coupled to a chemically reacting flow system. Nevertheless, they are of enough accuracy for giving blending criteria associated with main ash-related issues and for providing plant operators a sustainable fuel management. This allows prescribing this approach as the main guideline for blending design in a multiproduct MCP. However, more research is needed to asses this method in rate- or kinetically-controlled systems.

Interest disclosure

The authors declare no competing financial interest.

References

Aragon, G., Sanz, D., Mugica, I., Rojas, E., Larrion, M., Rodriguez Maroto, J., Ramos, R., Escalada, R., Borjabad, E., Gutierrez-Canas, C., 2015. Enhanced control of fine particle emissions from waste biomass combustion using a hybrid filter. Energy Fuels 29, 2358–2371. https://doi.org/10.1021/ef502825a.

ASTM D-2361-95, 2001. Standard Test Method for Chlorine in Coal.

ASTM E870-82, 2013. Standard Test Methods for Analysis of Wood Fuels. 10.1520/E0870.

Boström, D., Eriksson, G., Boman, C., Öilman, M., 2009. Ash transformations in fluidized-bed combustion of rapeseed meal. Energy Fuels 23, 2700–2706. https://doi.org/10.1021/ef800965b.

Boström, D., Grimm, A., Boman, C., Björnbom, E., Öhman, M., 2009. Influence of kaolin and calcite additives on ash transformations in small-scale combustion of oat. Energy Fuels 23, 5184–5190. https://doi.org/10.1021/ef900429f.

Boström, D., Skoglund, N., Grimm, A., Boman, C., Öhman, M., Broström, M., Backman, R., 2012. Ash transformation chemistry during combustion of biomass. Energy Fuels 26, 85–93. https://doi.org/10.1021/ef201205b.

Cuenca, J., Rodríguez, J., Martín-Morales, M., Sánchez-Roldán, Z., Zamorano, M., 2013. Effects of olive residue biomass fly ash as filler in self-compacting concrete. Constr. Build. Mater. 40, 702–709. https://doi.org/10.1016/j.conbuildmat.2012.09.101.

Davidsson, K.O., Åmand, L.E., Steenari, B.M., Elled, A.L., Eskilsson, D., Leckner, B., 2008. Countermeasures against alkali-related problems during combustion of biomass in a circulating fluidized bed boiler. Chem. Eng. Sci. 63, 5314–5329. https://doi.org/10.1016/j.ces.2008.07.012.

Davies, R.H., Dinsdale, A.T., Gisby, J.A., Robinson, J.A.J., Martin, S.M., 2002. MTDATA-thermodynamic and phase equilibrium software from the national physical laboratory. Calphad 26, 229–271. https://doi.org/10.1016/S0364-5916(02)00036-6.

Directive (EU) 2015/2193, n.d. On the Limitation of Emissions of Certain Pollutants into the Air from Medium Combustion Plants.

Doshi, V., Vuthaluru, H.B., Korbee, R., Kiel, J.H.A., 2009. Development of a modeling approach to predict ash formation during co-firing of coal and biomass. Fuel Process. Technol. 90, 1148–1156. https://doi.org/10.1016/j.fuproc.2009.05.019.

Elled, A.L., Davidsson, K.O., Åmand, L.E., 2010. Sewage sludge as a deposit inhibitor when co-fired with high potassium fuels. Biomass Bioenergy 34, 1546–1554. https://doi.org/10.1016/j.biombioe.2010.05.003.

EN 14774-2, 2009. Solid Biofuels - Determination of Moisture Content - Oven Dry Method - Part 2: Total Moisture. Simplified Method.

EN 14775, 2009. Solid Biofuels - Determination of Ash Content.

EN 14918, 2009. Solid Biofuels - Determination of Calorific Value.

EN 15104, 2011. Determination of Total Content of Carbon, Hydrogen and Nitrogen - Instrumental Methods.

EN 15148, 2009. Solid Biofuels - Determination of the Content of Volatile Matter.

EN 15289, 2011. Solid Biofuels - Determination of Total Content of Sulfur and Chlorine.
EN 15290, 2011. Solid Biofuels - Determination of Major Elements - Al, Ca, Fe, Mg, P, K, Si, Na and Ti.
FAOSTAT, 2009. SUA Crops Primary 2009 (WWW Document).
Fernández Llorente, M.J., Carrasco García, J.E., 2005. Comparing methods for predicting the sintering of biomass ash in combustion. Fuel 84, 1893–1900. https://doi.org/10.1016/j.fuel.2005.04.010.
Fernández Llorente, M.J., Escalada Cuadrado, R., Murillo Laplaza, J.M., Carrasco García, J.E., 2006. Combustion in bubbling fluidised bed with bed material of limestone to reduce the biomass ash agglomeration and sintering. Fuel 85, 2081–2092. https://doi.org/10.1016/j.fuel.2006.03.018.
García, R., Pizarro, C., Lavín, A.G., Bueno, J.L., 2012. Characterization of Spanish biomass wastes for energy use. Bioresour. Technol. 103, 249–258. https://doi.org/10.1016/j.biortech.2011.10.004.
GB/T 212, 2001. Proximate Analysis of Coal.
Gilbe, C., Lindström, E., Backman, R., Samuelsson, R., Burvall, J., Öhman, M., 2008. Predicting slagging tendencies for biomass pellets fired in residential appliances: a comparison of different prediction methods. Energy Fuels 22, 3680–3686. https://doi.org/10.1021/ef800321h.
Goñi, C., Helle, S., Garcia, X., Gordon, A., Parra, R., Kelm, U., Jimenez, R., Alfaro, G., 2003. Coal blend combustion: fusibility ranking from mineral matter composition. Fuel 82, 2087–2095. https://doi.org/10.1016/S0016-2361(03)00156-X.
Grimm, A., Skoglund, N., Boström, D., Boman, C., Öhman, M., 2012. Influence of phosphorus on alkali distribution during combustion of logging residues and wheat straw in a bench-scale fluidized bed. Energy Fuels 26, 3012–3023. https://doi.org/10.1021/ef300275e.
Grimm, A., Skoglund, N., Boström, D., Öhman, M., 2011. Bed agglomeration characteristics in fluidized quartz bed combustion of phosphorus-rich biomass fuels. Energy Fuels 25, 937–947. https://doi.org/10.1021/ef101451e.
Hansen, S.B., Jensen, P.A., Frandsen, F.J., Wu, H., Bashir, M.S., Wadenbäck, J., Sander, B., Glarborg, P., 2014. Deposit probe measurements in large biomass-fired grate boilers and pulverized-fuel boilers. Energy Fuels 28, 3539–3555. https://doi.org/10.1021/ef500442z.
Hu, Y., Cheng, S., Sun, P., Xie, J., Zhang, H., 2011. Research on fusion behavior of ash from mixedly burning biomass with coal. Therm. Power Gen. 40, 8–12.
Hubbard, C.R., Snyder, R.L., 1988. RIR - measurement and use in quantitative XRD. Powder Diffr. 3, 74–77. https://doi.org/10.1017/S0885715600013257.
Hupa, M., 2005. Interaction of fuels in co-firing in FBC. Fuel 84, 1312–1319. https://doi.org/10.1016/j.fuel.2004.07.018.
ISO 540, 2008. Hard Coal and Coke -- Determination of Ash Fusibility.
Jenkins, B.M., Baxter, L.L., Miles, T.R., 1998. Combustion properties of biomass. Fuel Process. Technol. 54, 17–46. https://doi.org/10.1016/S0378-3820(97)00059-3.
Jiménez, S., Ballester, J., 2005. Influence of operating conditions and the role of sulfur in the formation of aerosols from biomass combustion. Combust. Flame 140, 346–358. https://doi.org/10.1016/j.combustflame.2004.12.004.
Johansen, J.M., Jakobsen, J.G., Frandsen, F.J., Glarborg, P., 2011. Release of K, Cl, and S during pyrolysis and combustion of high-chlorine biomass. Energy Fuels 25, 4961–4971. https://doi.org/10.1021/ef201098n.
Karlsson, S., Åmand, L.-E., Liske, J., 2015. Reducing high-temperature corrosion on high-alloyed stainless steel superheaters by co-combustion of municipal sewage sludge in a fluidised bed boiler. Fuel 139, 482–493. https://doi.org/10.1016/j.fuel.2014.09.007.
Kassman, H., Pettersson, J., Steenari, B.M., Åmand, L.E., 2013. Two strategies to reduce gaseous KCl and chlorine in deposits during biomass combustion - injection of ammonium sulphate and co-combustion with peat. Fuel Process. Technol. 105, 170–180. https://doi.org/10.1016/j.fuproc.2011.06.025.
Khadilkar, A.B., Rozelle, P.L., Pisupati, S.V., 2016. Review of particle physics and chemistry in fluidized beds for development of comprehensive ash agglomeration prediction models. Energy Fuels 30, 3714–3734. https://doi.org/10.1021/acs.energyfuels.6b00079.
Knudsen, J.N., Jensen, P.a., Dam-Johansen, K., 2004. Quantification of the release of Cl, K and S to the gas phase from combustion of annual biomass. Prepr. Pap. - Am. Chem. Soc. Div. Fuel Chem. 49, 93–94.
Li, H., Han, K., Wang, Q., Lu, C., 2015. Influence of ammonium phosphates on gaseous potassium release and ash-forming characteristics during combustion of biomass. Energy Fuels 29, 2555–2563. https://doi.org/10.1021/acs.energyfuels.5b00285.
Li, L., Ren, Q., Li, S., Lu, Q., 2013. Effect of Phosphorus on the Behavior of Potassium during the Co-combustion of Wheat Straw with Municipal Sewage Sludge.
Li, Q.H., Zhang, Y.G., Meng, A.H., Li, L., Li, G.X., 2013. Study on ash fusion temperature using original and simulated biomass ashes. Fuel Process. Technol. 107, 107–112. https://doi.org/10.1016/j.fuproc.2012.08.012.
Lindström, E., Sandström, M., Boström, D., Öhman, M., 2007. Slagging characteristics during combustion of cereal grains rich in phosphorus. Energy Fuels 21, 710–717. https://doi.org/10.1021/ef060429x.
Magdziarz, A., Wilk, M., Gajek, M., Nowak-Wozny, D., Kopia, A., Kalemba-Rec, I., Kozinski, J.A., 2016. Properties of ash generated during sewage sludge combustion: a multifaceted analysis. Energy 113, 85–94. https://doi.org/10.1016/j.energy.2016.07.029.
Miller, B., Dugwell, D.R., Kandiyoti, R., 2003. The influence of injected HCl and SO_2 on the behavior of trace elements during wood-bark combustion. Energy Fuels 17, 1382–1391. https://doi.org/10.1021/ef030020x.
Miller, B.B., Dugwell, D.R., Kandiyoti, R., 2002. Partitioning of trace elements during the combustion of coal and biomass in a suspension-firing reactor. Fuel 81, 159–171. https://doi.org/10.1016/S0016-2361(01)00134-X.
Miller, B.B., Kandiyoti, R., Dugwell, D.R., 2002. Trace element emissions from co-combustion of secondary fuels with coal: a comparison of bench-scale experimental data with predictions of a thermodynamic equilibrium model. Energy Fuels 16, 956–963. https://doi.org/10.1021/ef0200065.
Moradian, F., Pettersson, A., Richards, T., 2015. Thermodynamic equilibrium model applied to predict the fouling tendency in a commercial fluidized-bed boiler, combusting solid waste. Energy Fuels 29, 3483–3494. https://doi.org/10.1021/acs.energyfuels.5b00346.
Niu, Y., Du, W., Tan, H., Xu, W., Liu, Y., Xiong, Y., Hui, S., 2013. Further study on biomass ash characteristics at elevated ashing temperatures: the evolution of K, Cl, S and the ash fusion characteristics. Bioresour. Technol. 129, 642–645. https://doi.org/10.1016/j.biortech.2012.12.065.
Niu, Y., Tan, H., Hui, S., 2016. Ash-related issues during biomass combustion: Alkali-induced slagging, silicate melt-induced slagging (ash fusion), agglomeration, corrosion, ash utilization, and related countermeasures. Prog. Energy Combust. Sci. 52, 1–61. https://doi.org/10.1016/j.pecs.2015.09.003.
Nutalapati, D., Gupta, R., Moghtaderi, B., Wall, T.F., 2007. Assessing slagging and fouling during biomass combustion: a thermodynamic approach allowing for alkali/ash reactions. Fuel Process. Technol. 88, 1044–1052. https://doi.org/10.1016/j.fuproc.2007.06.022.
Piispanen, M.H., Niemelä, M.E., Tiainen, M.S., Laitinen, R.S., 2012. Prediction of bed agglomeration propensity directly from solid biofuels: a look behind fuel indicators. Energy Fuels 26, 2427–2433. https://doi.org/10.1021/ef300173w.
Piotrowska, P., Grimm, A., Skoglund, N., Boman, C., Öhman, M., Zevenhoven, M., Boström, D., Hupa, M., 2012. Fluidized-bed combustion of mixtures of rapeseed cake and bark: the resulting bed agglomeration characteristics. Energy Fuels 26, 2028–2037. https://doi.org/10.1021/ef300130e.
Piotrowska, P., Zevenhoven, M., Davidsson, K., Hupa, M., Åmand, L.-E., Barišić, V., Coda Zabetta, E., 2010. Fate of alkali metals and phosphorus of rapeseed cake in circulating fluidized bed boiler part 2: cocombustion with coal. Energy Fuels 24, 4193–4205. https://doi.org/10.1021/ef100482n.
Poole, D., Argent, B.B., Sharifi, V.N., Swithenbank, J., 2008. Prediction of the distribution of alkali and trace elements between the condensed and gaseous phases in a municipal solid waste incinerator. Fuel 87, 1318–1333. https://doi.org/10.1016/j.fuel.2007.07.017.
Pronobis, M., 2005. Evaluation of the influence of biomass co-combustion on boiler furnace slagging by means of fusibility correlations. Biomass Bioenergy 28, 375–383. https://doi.org/10.1016/j.biombioe.2004.11.003.
Red Española de compostaje, E.P.S.A., 2015. Residuos orgánicos y agricultura intensiva III.
Ren, Q., Li, L., 2015. Co-combustion of agricultural straw with municipal sewage sludge in a fluidized bed: role of phosphorus in potassium behavior. Energy Fuels 29, 4321–4327. https://doi.org/10.1021/acs.energyfuels.5b00790.
Skoglund, N., Grimm, A., Öhman, M., Boström, D., 2013. Effects on ash chemistry when co-firing municipal sewage sludge and wheat straw in a fluidized bed: influence on the ash chemistry by fuel mixing. Energy Fuels 27, 5725–5732. https://doi.org/10.1021/ef401197q.
Skrifvars, B.-J., Backman, R., Hupa, M., 1998. Characterization of the sintering tendency of ten biomass ashes in FBC conditions by a laboratory test and by phase equilibrium calculations. Fuel Process. Technol. 56, 55–67. https://doi.org/10.1016/S0378-3820(97)00084-2.
Spinelli, R., Picchi, G., 2010. Industrial harvesting of olive tree pruning residue for energy biomass. Bioresour. Technol. 101, 730–735. https://doi.org/10.1016/j.biortech.2009.08.039.
Steenari, B.-M., Lindqvist, O., 1998. High-temperature reactions of straw ash and the anti-sintering additives kaolin and dolomite. Biomass Bioenergy 14, 67–76. https://doi.org/10.1016/S0961-9534(97)00035-4.
Steenari, B.-M., Lundberg, A., Pettersson, H., Wilewska-Bien, M., Andersson, D., 2009. Investigation of ash sintering during combustion of agricultural residues and the effect of additives. Energy Fuels 23, 5655–5662. https://doi.org/10.1021/ef900471u.
Teixeira, P., Lopes, H., Gulyurtlu, I., Lapa, N., Abelha, P., 2012. Evaluation of slagging and fouling tendency during biomass co-firing with coal in a fluidized bed. Biomass Bioenergy 39, 192–203. https://doi.org/10.1016/j.biombioe.2012.01.010.
Thy, P., Jenkins, B., Grundvig, S., Shiraki, R., Lesher, C., 2006. High temperature elemental losses and mineralogical changes in common biomass ashes. Fuel 85, 783–795. https://doi.org/10.1016/j.fuel.2005.08.020.
Thy, P., Lesher, C., Jenkins, B., 2000. Experimental determination of high-temperature elemental losses from biomass slag. Fuel 79, 693–700. https://doi.org/10.1016/S0016-2361(99)00195-7.
UNE 32024, 1995. Solid Mineral Fuels. Determinacion of Chlorine using Eschka Mixture.

Vamvuka, D., Pitharoulis, M., Alevizos, G., Repouskou, E., Pentari, D., 2009. Ash effects during combustion of lignite/biomass blends in fluidized bed. Renew. Energy 34, 2662–2671. https://doi.org/10.1016/j.renene.2009.05.005.

Vamvuka, D., Zografos, D., Alevizos, G., 2008. Control methods for mitigating biomass ash-related problems in fluidized beds. Bioresour. Technol. 99, 3534–3544. https://doi.org/10.1016/j.biortech.2007.07.049.

Van Caneghem, J., Brems, A., Lievens, P., Block, C., Billen, P., Vermeulen, I., Dewil, R., Baeyens, J., Vandecasteele, C., 2012. Fluidized bed waste incinerators: design, operational and environmental issues. Prog. Energy Combust. Sci. 38, 551–582. https://doi.org/10.1016/j.pecs.2012.03.001.

Vassilev, S.V., Baxter, D., Andersen, L.K., Vassileva, C.G., 2010. An overview of the chemical composition of biomass. Fuel 89, 913–933. https://doi.org/10.1016/j.fuel.2009.10.022.

Vassilev, S.V., Baxter, D., Andersen, L.K., Vassileva, C.G., 2013. An overview of the composition and application of biomass ash. Fuel 105, 19–39. https://doi.org/10.1016/j.fuel.2012.10.001.

Vassilev, S.V., Baxter, D., Vassileva, C.G., 2014. An overview of the behaviour of biomass during combustion: part II. Ash fusion and ash formation mechanisms of biomass types. Fuel 117, 152–183. https://doi.org/10.1016/j.fuel.2013.09.024.

Vassilev, S.V., Baxter, D., Vassileva, C.G., 2013. An overview of the behaviour of biomass during combustion: part I. Phase-mineral transformations of organic and inorganic matter. Fuel 112, 391–449. https://doi.org/10.1016/j.fuel.2013.05.043.

Vassilev, S.V., Vassileva, C.G., Vassilev, V.S., 2015. Advantages and disadvantages of composition and properties of biomass in comparison with coal: an overview. Fuel 158, 330–350. https://doi.org/10.1016/j.fuel.2015.05.050.

Wang, L., Hustad, J.E., Skreiberg, , Skjevrak, G., Grønli, M., 2012. A critical review on additives to reduce ash related operation problems in biomass combustion applications. Energy Procedia 20, 20–29. https://doi.org/10.1016/j.egypro.2012.03.004.

Wang, L., Skjevrak, G., Hustad, J.E., Gronli, M.G., 2011. Effects of sewage sludge and marble sludge addition on slag characteristics during wood waste pellets combustion. Energy Fuels 25, 5775–5785. https://doi.org/10.1021/ef2007722.

Wiinikka, H., Gebart, R., Boman, C., Boström, D., Öhman, M., 2007. Influence of fuel ash composition on high temperature aerosol formation in fixed bed combustion of woody biomass pellets. Fuel 86, 181–193. https://doi.org/10.1016/j.fuel.2006.07.001.

Xiao, R., Chen, X., Wang, F., Yu, G., 2011. The physicochemical properties of different biomass ashes at different ashing temperature. Renew. Energy 36, 244–249. https://doi.org/10.1016/j.renene.2010.06.027.

Xiong, S., Burvall, J., Örberg, H., Kalen, G., Thyrel, M., Öhman, M., Boström, D., Örberg, H., Kalen, G., Thyrel, M., Öhman, M., Boström, D., 2008. Slagging characteristics during combustion of corn stovers with and without kaolin and calcite. Energy Fuels 22, 3465–3470. https://doi.org/10.1021/ef700718j.

Zevenhoven-Onderwater, M., Blomquist, J., Skrifvars, B., Backman, R., Hupa, M., 2000. The Prediction of Behaviour of Ashes from Five Different Solid Fuels.pdf 79, 1353–1361.